- E.-D. Schulze, Carbon and Nitrogen Cycling in European Forest Ecosystems (Springer Verlag, Berlin, 2000)
- D. D. Baldocchi, B. B. Hicks, T. P. Meyers, *Ecology* 69, 1331 (1988).
- 13. R. Valentini et al., Nature 404, 861 (2000).
- D. Papale, R. Valentini, Global Change Biol., 9, 525 (2003).
- C. A. Mucher, PELCOM, Pan-European Land Use and Land Cover Monitoring (ALTERRA, Wageningen, 2000); available online at www.geo-informatie.nl/ cgi/projects/eu/pelcom/index.htm.
- 16. G.-J. Nabuurs, thesis, University of Joensuu, Finland (2001).
- T. Häme et al., AVHRR-Based Forest Probability Map of the Pan-European Area (Joint Research Centre, Ispra, Italy, 1999).
- A. I. Pisarenko et al., Development of Forest Resources in the European Part of the Russian Federation (European Forest Institute, Joensuu, Finland, 2000).
- 19. A. Shvidenko, S. Nilsson, Clim. Change 55, 5 (2002).
- 20. S. W. Pacala et al., Science 292, 2316 (2001).
- R. B. Jackson, J. L. Banner, E. G. Jobbágy, W. T. Pockman, D. H. Wall, *Nature* 418, 623 (2002).
- 22. P. Smith, D. S. Powlson, J. U. Smith, P. D. Falloon, K. Coleman, *Global Change Biol.* **6**, 525 (2000).
- 23. L. M. Vleeshouwers, A. Verhagen, *Global Change Biol.* **8**, 519 (2002).
- The Food and Agricultural Organization statistical databases are available online at www.fao.org/ waicent/portal/statistics\_en.asp.
- 25. S. Sleutel, S. De Neve, G. Hofman, *Soil Use Manag.*, in press
- G. Dersch, K. Boehm, in Bodenschutz in Österreich, W. E. H. Blum, E. Klaghofer, A. Loechl, P. Ruckenbauer, Eds. (Bundesamt und Forschungszentrum fuer Landwirtschaft, Österreich, Germany, 1997), pp. 411–432.
- 27. R. Milne, R. Tomlinson, J. Gauld in UK Emissions by Sources and Removals by Sinks due to Land Use, Land Use Change and Forestry Activities (April 2001 report to Department for Environment, Food, and Rural Affairs, London, 2001); available online at www. nbu.ac.uk/ukcarbon/.
- 28. T. V. Armentano, E. S. Menges, *J. Ecol.* **74**, 755 (1986).
- M. S. Botch, K. I. Kobak, T. S. Vinson, T. P. Kolchugina, Global Biogeochem. Cycles 9, 37 (1995).
- E. Lappalainen, Global Peat Resources (International Peat Society, Jyskä, Finland, 1996).
- T. V. Armentano, J. T. A. Verhoeven, in Wetlands and Shallow Continental Water Bodies, B. C. Patten et al., Eds. (SPB Academic Publishing, The Hague, 1990), pp. 281–311.
- 32. P. Bousquet et al., Science **290**, 1342 (2000).
- T. Kaminski, M. Heimann, R. Giering, J. Geophys. Res. 104, 18555 (1999).
- P. Bousquet, P. Ciais, P. Peylin, M. Ramonet, P. Monfrey, J. Geophys. Res. 104, 26161 (1999).
- J. Penman et al., in IPCC Good Practice Guidance and Uncertainty Management in National Greenhouse Gas Inventories, J. Penman et al., Eds. (IPCC National Greenhouse Gas Inventories Programme, Institute for Global Environmental Strategies, Hayama, Japan, 2000); available online at www.ipcc-nggip. iges.or.ip/.
- 36. J. G. J. Olivier et al., Env. Sci. Pol. 2, 241 (1999).
- J. G. J. Olivier, thesis, University of Utrecht, Netherlands (2002).
- 38. A. Günther et al., J. Geophys. Res. **100**, 8873 (1995).
- 39. Data can be found online at www.efi.fi/efidas/.
- G.-J. Nabuurs, R. Paivinen, R. Sikkema, G. M. J. Mohren, *Biomass Bioenergy* 13, 345 (1997).
- 41. R. F. Stallard, Global Biogeochem. Cycles 12, 231 (1998).
- 42. W. Ludwig, J.-L. Probst, Am. J. Sci. 298, 265 (1998).
- 43. M. Frankignoulle *et al., Science* **282**, 434 (1998). 44. The Edgar database is available online at http://
- The Edgar database is available online at http:// arch.rivm.nl/env/int/coredata/edgar/index.html.
   E.-D. Schulze, C. Wirth, M. Heimann, Science 289,
- 2058 (2000).46. A. Freibauer, M. D. A. Rounsevell, P. Smith, A. Verhagen, *Soil Sci. Rev.*, in press.
- P. M. Cox, R. A. Betts, C. D. Jones, S. A. Spall, I. J. Totterdell, *Nature* 408, 184 (2000).

- E.-D. Schulze, M. Heimann, in Asian Change in the Context of Global Change, J. N. Galloway, J. Melillo, Eds. (Cambridge Univ. Press, Cambridge, 1998), pp. 145
- P. J. Rayner, I. G. Enting, R. J. Francey, R. Langenfelds, Tellus 51B, 213 (1999).
- The authors acknowledge the contributions of P. G. Jarvis (U.K.), M. Heimann, J. Liski and K. Pingoud (Finland), D. Papale (Italy), J.-F. Soussana, P. Bousquet (France), and J. Verhagen and R. van den Bos (Neth-

erlands). I.A.J. is a postdoctoral researcher of the Fund for Scientific Research, Flanders (F.W.O.).

# **Supporting Online Material**

www.sciencemag.org/cgi/content/full/1083592/DC1 Materials and Methods

18 February 2003; accepted 6 May 2003 Published online 22 May 2003; 10.1126/science.1083592 Include this information when citing this paper.

# Sensing DNA Damage Through ATRIP Recognition of RPA-ssDNA Complexes

Lee Zou<sup>1,2</sup> and Stephen J. Elledge<sup>1,2,3</sup>\*

The function of the ATR (ataxia-telangiectasia mutated— and Rad3-related)—ATRIP (ATR-interacting protein) protein kinase complex is crucial for the cellular response to replication stress and DNA damage. Here, we show that replication protein A (RPA), a protein complex that associates with single-stranded DNA (ssDNA), is required for the recruitment of ATR to sites of DNA damage and for ATR-mediated Chk1 activation in human cells. In vitro, RPA stimulates the binding of ATRIP to ssDNA. The binding of ATRIP to RPA-coated ssDNA enables the ATR-ATRIP complex to associate with DNA and stimulates phosphorylation of the Rad17 protein that is bound to DNA. Furthermore, Ddc2, the budding yeast homolog of ATRIP, is specifically recruited to double-strand DNA breaks in an RPA-dependent manner. A checkpoint-deficient mutant of RPA, rfa1-t11, is defective for recruiting Ddc2 to ssDNA both in vivo and in vitro. Our data suggest that RPA-coated ssDNA is the critical structure at sites of DNA damage that recruits the ATR-ATRIP complex and facilitates its recognition of substrates for phosphorylation and the initiation of checkpoint signaling.

The ATR (ATM- and Rad3-related) protein kinase plays a central role in the cellular response to replication stress and DNA damage such as double-strand breaks (DSBs) (1, 2). In response to these events, ATR phosphorylates substrates such as p53, Brca1, Chk1, and Rad17. The phosphorylation of ATR substrates collectively inhibits DNA replication and mitosis and promotes DNA repair, recombination, or apoptosis. Despite the identification of many effectors of ATR, the mechanism by which ATR is activated by replication stress or DNA damage remains unsolved.

In human cells, ATR exists in a stable complex with ATRIP (ATR-interacting protein), a potential regulatory partner (3). Mec1 and Rad3, the budding and fission yeast homologs of ATR, respectively, also form similar complexes with Ddc2 (also called Lcd1 or Pie1) and Rad26, respectively (4–7). In budding yeast, the Mec1-Ddc2 complex is

recruited to DSBs induced by the HO endonuclease (HO) or single-stranded DNA (ssDNA) at telomeres caused by a mutation in Cdc13. The recruitment of Mec1-Ddc2 to sites of DNA damage is independent of the replication factor C (RFC)-like protein Rad24 and the proliferating cell nuclear antigen (PCNA)-like proteins Ddc1, Mec3, and Rad17 (8, 9). Likewise, ATR localization to DNA damage-induced foci does not require human Rad17, the homolog of yeast Rad24 (10). Thus, the ATR-ATRIP and Mec1-Ddc2 complexes might recognize certain DNA or DNA-protein structures at damage sites in the absence of the RFC-like and PCNA-like checkpoint complexes.

Many distinct DNA damaging agents can elicit the DNA damage or stress response that is mediated by ATR. Thus, a central question in checkpoint signaling is whether there is a sensor for each type of damage or whether all of these are converted to a common intermediate that is detected by a single sensor. A plausible candidate for a common intermediate is ssDNA. In yeast, ssDNA is present at telomeres because of the loss of function of Cdc13 and at the sites of damage caused by HO-induced breaks (11, 12). It has been proposed as a requirement for strong and sustained activation of the checkpoint (13).

<sup>&</sup>lt;sup>1</sup>Verna & Marrs McLean Department of Biochemistry and Molecular Biology, <sup>2</sup>Howard Hughes Medical Institute, <sup>3</sup>Department of Molecular and Human Genetics, Baylor College of Medicine, Houston, TX 77030, USA.

<sup>\*</sup>To whom correspondence should be addressed. E-mail: selledge@bcm.tmc.edu

ssDNA does not exist naked in the cell, but is coated by replication protein A (RPA), a ssDNA-binding protein complex (14). RPA has been implicated in the checkpoint response in several ways. First, RPA is an effector of the DNA damage checkpoint, because two subunits of the yeast RPA complex, Rpa1 and Rpa2, are phosphorylated in response to DNA damage and treatments that block replication (15, 16). Second, certain yeast RPA mutants have been shown to adapt more quickly from the cell-cycle arrest induced by DNA damage (12) and to show defects in arresting the cell cycle (17, 18). However, it is unclear whether these effects are due to RPA's role as an effector of the pathway or whether it might function in signal generation. Thus, we investigated whether RPA takes part in damage recognition, activation of the ATR-ATRIP complex, or both processes.

RPA is required for the formation of nuclear foci that contain ATR-ATRIP. ATR, but not the related protein kinase ATM (ataxia-telangiectasia mutated), is activated in cells exposed to ultraviolet radiation (UV). To investigate whether ssDNA is generated by UV-induced damage, we isolated chromatin from undamaged or UV-damaged human cells and examined the association of RPA with chromatin. After UV treatment, an increased amount of RPA34, the second largest subunit of RPA, was detected on chromatin (Fig. 1A). Thus, it appears that more ssDNA is generated after UV damage and that the ssDNA generated becomes coated by RPA.

RPA localizes to nuclear foci upon DNA damage (19). ATR and ATRIP also localize to nuclear foci after DNA damage (3, 20). To determine whether RPA colocalizes with the ATR-ATRIP complex after damage, we examined the localization of RPA and ATR-ATRIP in undamaged cells and cells treated with ionizing radiation (IR). Two hours after treatment of cells with IR, RPA and ATR formed nuclear foci that were not observed in undamaged cells (Fig. 1B). The damage-induced RPA foci completely colocalized with the ATR foci (Fig. 1B). Similar results were seen for RPA and ATRIP (21). Thus RPA and the ATR-ATRIP complex appear to be recruited to the same sites of DNA damage in vivo.

To determine whether RPA is required for the activation of ATR-mediated DNA damage signaling in human cells, we used small interfering RNA (siRNA) to specifically inhibit the expression of RPA70, the largest subunit of RPA. The amount of RPA70 protein was substantially reduced in the siRNA-transfected HeLa cells 3 days after transfection (Fig. 1C), whereas amounts of several other checkpoint proteins showed little alteration.

To investigate whether RPA is required for the recruitment of ATR-ATRIP to damage-

induced foci, we examined the localization of ATR and ATRIP in cells transfected with control green fluorescent protein (GFP) siRNA or RPA70 siRNA. Two hours after treatment of cells with IR, ATR foci were detected in 27% of the cells transfected with control siRNA. In contrast, only 4% of the cells transfected with RPA70 siRNA displayed IR-induced ATR foci. The fraction of RPA70 siRNA-transfected cells that displayed IR-induced foci that contained ATRIP was similarly reduced compared to that in controls. Representative samples of the cells transfected with control siRNA or RPA70 siRNA are shown in Fig. 1D. The small fraction of the RPA70 siRNA-treated cells that displayed ATR- or ATRIP-containing foci retained higher amounts of RPA than did other cells in the same population (21). Thus, the recruitment of ATR and ATRIP to the damageinduced nuclear foci is dependent upon RPA.

RPA is required for the activation of Chk1. The recruitment of ATR-ATRIP to DNA damage is thought to be required for its role in the activation of checkpoint signaling (1, 2). A key substrate of ATR-ATRIP is the human Chk1 protein kinase, which is phosphorylated by ATR on Ser<sup>345</sup> in response to DNA damage or replication blocks (10, 22). The damage-induced phosphorylation of Chk1

can be detected with antibodies that specifically recognize Chk1 phosphorylated on Ser345 (22). Thus, we examined the dependency of Chk1 activation on RPA. In HeLa cells transfected with RPA70 siRNA, phosphorylation of Chk1 induced by hydroxyurea (HU) was diminished (by three-quarters) compared to control cells (Fig. 2A). Furthermore, the phosphorylation of Chk1 induced by UV was also reduced when the expression of RPA was inhibited with siRNA (Fig. 2B). To test whether this RPA dependency is cell line-specific, we also examined Chk1 phosphorylation in U2OS cells in response to various doses of UV. Although amounts of RPA were constant in HeLa cells, the amounts of RPA in U20S cells increased in response to DNA damage. In U2OS cells transfected with control siRNA, Chk1 was efficiently phosphorylated in response to UV, but this phosphorylation was reduced in cells treated with siRNA to RPA (Fig. 2C). The greatest decreases were observed at the highest doses of UV. There may be residual RPA in these cells sufficient to recognize the small amounts of ssDNA produced at low UV doses. These results suggest that RPA regulates activation of ATR not only in response to replication blocks but also in response to DNA damage.

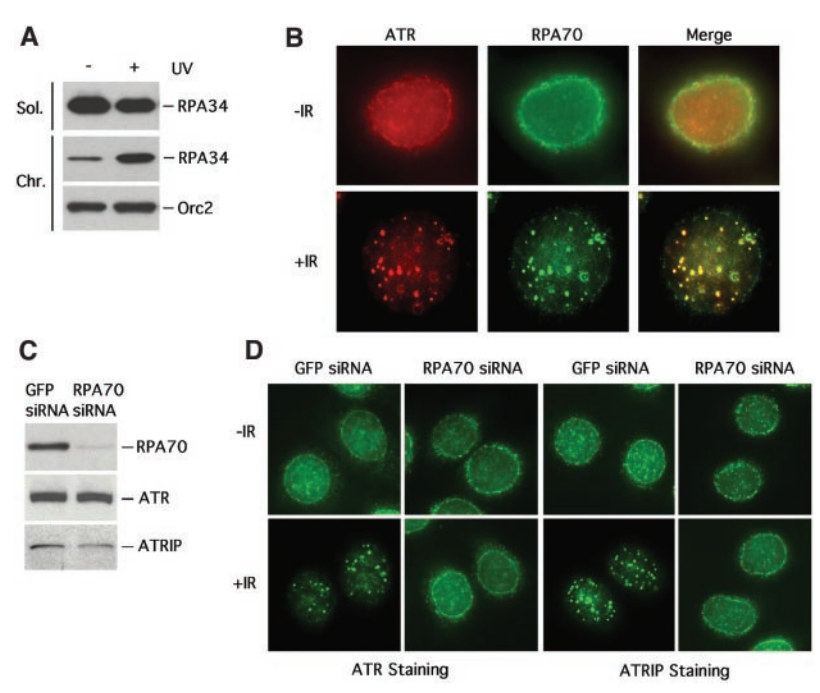
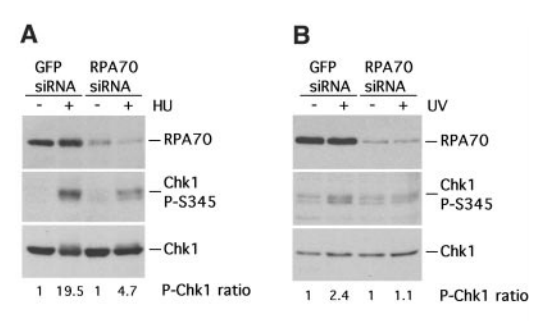


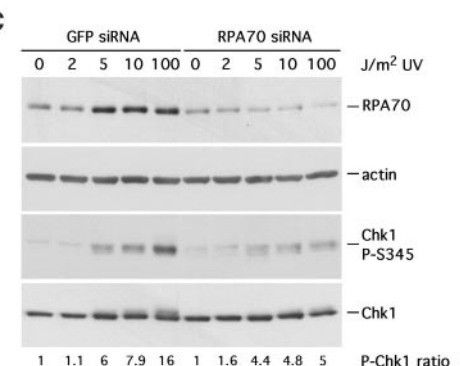
**Fig. 1.** Colocalization of RPA with the ATR-ATRIP complex after damage and the requirement of RPA for the formation of foci that contain ATR-ATRIP. (**A**) HCT116 cells were left untreated or were treated with 50 J/m<sup>2</sup> of UV, then subjected to chromatin fractionation after 2 hours (10). RPA34 and Orc2 in the indicated fractions were detected by immunoblotting. Sol, soluble fractions; Chr, chromatin fractions. Orc2 served as a loading control for the chromatin fractions. (**B**) HeLa cells were left untreated or were treated with 10 gray (Gy) of IR. Two hours after IR treatment, cells were briefly extracted with detergent, fixed in paraformaldehyde, and subjected to immunostaining with antibodies to ATR or RPA70. (**C**) HeLa cells were transfected twice with GFP siRNA or RPA70 siRNA, and cellular extracts were prepared 3 days after the first transfection. RPA70, ATR, and ATRIP in the extracts were detected by immunoblotting with the corresponding antibodies. (**D**) HeLa cells transfected with GFP siRNA or RPA70 siRNA were treated with 10 Gy of IR or left untreated. Two hours after IR treatment, cells were subjected to immunostaining with antibodies to ATR (left) or ATRIP (right) as in (B).

**RPA stimulates the binding of ATRIP to ssDNA.** The requirement of RPA for the recruitment of ATR-ATRIP to damage-induced

nuclear foci suggests that RPA might function in damage recognition, working to directly recruit ATR-ATRIP. We therefore tested whether

Fig. 2. Regulation of ATR-mediated phosphorylation of Chk1 by RPA. (A) HeLa cells transfected with GFP siRNA or RPA siRNA were treated with 1 mM HU for 24 hours or left untreated. The phosphorylation of Chk1 on Ser345 was monitored with the phosphospecific antibody to P-Ser<sup>345</sup> of Chk1 (P-S345). (B) HeLa cells were transfected as in (A), treated with 10 J/m<sup>2</sup> of UV, and collected after 2 hours. The phosphorylation of Chk1 on Ser<sup>345</sup> was detected as in (A). (C) U2OS cells were transfected as in (A), and treated with the indicated doses of UV. Cellular extracts were made 1 hour after the UV treatment. Amounts of RPA70, Chk1, and actin were analyzed with the corresponding antibodies. The phosphorylation of Chk1 was detected by the antibody to P-Ser<sup>345</sup> of





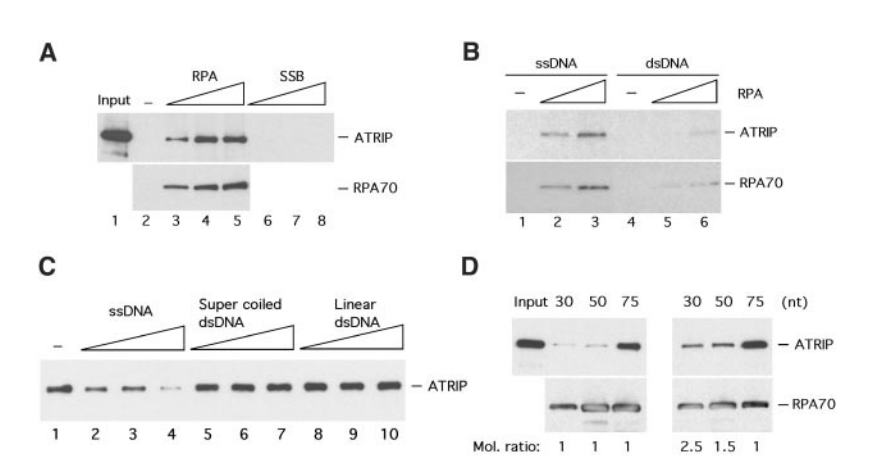


Fig. 3. Stimulation of ATRIP binding to ssDNA by RPA. (A) Recruitment of ATRIP to ssDNA by RPA. The biotinylated 75-nt oligomer (5 pmol) was attached to streptavidin-coated beads and incubated with various amounts of purified RPA or SSB (0, 1, 2.5, or 8 pmol). After a 30-min incubation, ATRIP (0.5 pmol) was added to the reactions and incubated for 30 min. The ssDNA oligomer was retrieved with streptavidin beads, and the unbound proteins were washed away. The ATRIP and RPA associated with ssDNA was detected by immunoblotting with the corresponding antibodies. Input, total input of ATRIP. (B) Preferential binding of ATRIP to ssDNA-RPA complexes. The biotinylated 75-nt oligomer was annealed with its complementary oligomer (unmodified) and the resultant dsDNA was attached to streptavidin beads. The ssDNA or dsDNA-coated beads were incubated with various amounts of RPA (0, 0.1, or 0.25 pmol) and then with 0.5 pmol of ATRIP as in (A). The ATRIP and RPA associated with DNA were detected by immunoblotting. A small fraction of the dsDNA may be single-stranded because of incomplete annealing. (C) Failure of dsDNA to compete for ATRIP binding. The biotinylated 75-nt oligomer (100 ng) was incubated with RPA in the presence of various amounts (0, 50, 100, or 250 ng) of single-stranded M13 DNA, supercoiled plasmid DNA (Bluescript), or Sma-I-linearized plasmid, and then incubated with ATRIP. The ATRIP bound to the biotinylated 75-nt oligomer was detected by immunoblotting. Lane 2 on this gel may be underloaded. (D) Enhanced ATRIP binding to longer ssDNA. Left: Equal moles (5 pmol) of the biotinylated 30-, 50-, or 75-nt oligomers were incubated with RPA and ATRIP as in (A). Right: Oligomers with equal masses of ssDNA (12.5 pmol of 30-nt oligomer, 7.5 pmol of 50-nt oligomer, or 5 pmol of 75-nt oligomer) were incubated with RPA and ATRIP as in (A). The ATRIP and RPA bound to DNA were detected by immunoblotting.

RPA could stimulate the binding of ATRIP or ATR to ssDNA in vitro. Human ATRIP protein was tagged with a Flag epitope, expressed in baculovirus-infected insect cells, and purified on an affinity column made with monoclonal antibodies to Flag. Purified ATRIP was incubated with biotinylated, single-stranded, 75-nucleotide (nt) DNA oligomers, either in the absence of RPA or in the presence of various amounts of bacterially expressed and purified RPA (23). In the absence of RPA, no ATRIP was associated with the ssDNA retrieved by streptavidin beads (Fig. 3A, lane 2). In the presence of RPA, however, ATRIP bound to ssDNA efficiently (Fig. 3A). Furthermore, the amounts of ssDNA-bound ATRIP were proportional to the amounts of RPA on the ssDNA (Fig. 3, A and B). In marked contrast, purified Escherichia coli ssDNA binding protein (SSB) did not stimulate binding of ATRIP to ssDNA (Fig. 3A). These results demonstrate that RPA enables ATRIP to bind to ssDNA. Similar results were obtained when 75-nt oligomers of a different sequence were tested (21), indicating that the binding of ATRIP to RPA-coated ssDNA does not require a specific DNA sequence or secondary structure.

The budding yeast ATRIP homolog Ddc2 is reported to bind to the ends of double-stranded DNA (dsDNA) (24). To test whether ATRIP also binds to dsDNA, we annealed the biotinylated ssDNA oligomer with its complementary oligomer and incubated the resultant dsDNA with purified ATRIP. ATRIP did not bind to dsDNA in the absence of RPA (Fig. 3B, lane 4). In the presence of RPA, both ATRIP and RPA bound more efficiently to ssDNA than to dsDNA (Fig. 3B). The small amounts of RPA and ATRIP that bound to dsDNA could be due to contaminating ssDNA. We also tested ssDNA from the single-stranded bacteriophage M13, supercoiled dsDNA, and linearized dsDNA as competitors in the ATRIP-RPAssDNA binding reactions. The competitors were incubated with biotinylated ssDNA, RPA, and ATRIP. Only the single-stranded M13 DNA inhibited binding of ATRIP to the biotinylated ssDNA (Fig. 3C). Hence, RPA confers upon ATRIP a higher affinity to ssDNA than to dsDNA or to the ends of dsDNA.

To determine whether the length of ssDNA is important for the binding of ATRIP, we compared the recruitment of ATRIP to biotinylated 30-, 50-, and 75-nt ssDNA oligomers in the presence of RPA. When equal moles of the three oligomers were used in the reactions, the 75-nt oligomer retrieved more ATRIP than did the two shorter oligomers (Fig. 3D). To determine whether this was due to a greater mass of ssDNA or to some form of cooperative binding to longer ssDNA, we increased the molar concentrations of the 30- and 50-nt oligomers in the reactions such that the total mass of ssDNA was equal for all three oligomers. As expected, similar amounts of RPA

were bound to all three oligomers (Fig. 3D). However, ATRIP bound much more efficiently to the 75-nt oligomer than to the shorter oligomers (Fig. 3D). These results indicate that the binding of ATRIP to RPA-coated ssDNA is length-dependent with a threshold length between 50 and 75 nt that renders ATRIP binding more efficient. The amount of DNA covered by each RPA complex is ~30 nt (14) and suggests that of the three templates, only the 75-nt fragment has the capability to efficiently bind two RPA complexes. Thus, loading of multiple RPAs onto longer ssDNA may stimulate the binding of ATRIP, and the binding of ATRIP to these longer templates might be cooperative. This could have important implications for ATR-ATRIP signal sensing.

RPA enables the ATR-ATRIP complex to associate with ssDNA. To further assess the biological significance of the RPAdependent interaction of ATRIP with ssDNA, we asked if RPA could stimulate the binding of the ATR-ATRIP complex to ssDNA. We first tested whether ATR itself could bind to ssDNA. Flag-tagged human ATR was overexpressed in 293T cells and affinity-purified (25). The majority of the purified ATR was not in association with ATRIP, because silver staining detected no ATRIP in this preparation (21). Unlike ATRIP, ATR bound to ssDNA in the absence of RPA (Fig. 4A). Such binding of ATR to ssDNA was not affected by the presence of RPA (Fig. 4A). Therefore, ATR itself may possess an affinity to ssDNA, but this affinity is not regulated by RPA in the absence of ATRIP.

To examine directly the binding of the ATR-ATRIP complex to ssDNA, we reconstituted the ATR-ATRIP complex by combining purified ATR and purified ATRIP. The amount of ATR bound to ssDNA was substantially reduced in the presence of ATRIP (Fig. 4A, lane 6). The small amount of ATR bound to ssDNA was apparently not in complex with ATRIP, because no ATRIP was found on the ssDNA molecules (Fig. 4A, lane 6). These results suggest that the affinity of ATR for ssDNA is obscured in the ATR-ATRIP complex and that the ATR-ATRIP complex and that the ATR-ATRIP complex cannot bind to ssDNA in the absence of RPA.

In the presence of RPA, the amounts of ATR-ATRIP complex that bound to ssDNA were increased (Fig. 4A, lane 7). Thus, RPA-coated ssDNA is sufficient to recruit ATR-ATRIP. The interaction between ATRIP and RPA-coated ssDNA likely plays a critical role in recruiting the ATR protein kinase to ssDNA. It is unclear how much of the ATR is complexed with ATRIP in this experiment, and some ATRIP might remain free after reconstitution of the ATR-ATRIP complex. The free ATRIP may be competing with the ATR-ATRIP complex, artificially reducing the amount of ATR brought down in lane 7.

The ability of free ATR to bind ssDNA suggested the possibility that ATR may be able to signal damage in the absence of ATRIP and RPA. To examine this, we measured the amount of free ATR in cells. Multiple rounds of immunoprecipitation with antibodies to ATRIP were performed, and the levels of ATR remaining in the extracts was measured (Fig. 4B). All detectable ATR (>95%) was depleted by immunoprecipitation of ATRIP (Fig. 4B), showing that the vast majority of ATR is present in complexes with ATRIP in human cells. This is also consistent with the genetics of these genes, because loss of ATRIP, DDC2, or rad26 abolishes the checkpoint responses of their respective organisms to the same degree as loss of ATR, MEC1, or rad3, respectively (3-5). Therefore, we feel that the ability of ATR to bind ssDNA is unlikely to play an important role in damage recognition in vivo and that ATR is likely to be recruited to damage sites through the interaction between ATRIP and RPA-coated ssDNA.

RPA stimulates the phosphorylation of Rad17 on DNA by ATR-ATRIP. To test whether recruitment of the ATR-ATRIP complex stimulates phosphorylation of ATR substrates on DNA, we tested the effects of RPA on the phosphorylation of Rad17 by ATR-ATRIP. Flag-tagged Rad17 was coexpressed with the four small subunits of RFC (Rfc2-5) in baculovirus-infected insect cells, and the Rad17-Rfc2-5 complex was purified (26). The Rad17-Rfc2-5 complex associated with ssDNA (Fig. 4C) (26). The phosphorylation of Rad17 was analyzed with a phosphospecific antibody to phosphorylated Ser<sup>635</sup> (P-Ser<sup>635</sup>), an in vitro and in vivo site of phosphorylation by ATR (Fig. 4C) (10, 27, 28). In the absence of RPA, the ssDNAbound Rad17 was not phosphorylated by ATR-ATRIP. In contrast, the ssDNA-bound Rad17 was clearly phosphorylated by ATR-ATRIP in the presence of RPA (Fig. 4C).

Although ssDNA-bound Rad17 can be phosphorylated by ATR-ATRIP in vitro, it is not clear whether ssDNA is the DNA structure recognized by the Rad17-Rfc2-5 complex in vivo. Moreover, the UV-induced phosphorylation of Rad17 by ATR in vivo requires the PCNA-like protein Hus1 (10), which was not present in our in vitro assays. However, it is unclear what role the Rad9-Rad1-Hus1 complex plays in vivo. It could make Rad17 an even better substrate by stimulating ATR or tethering it to DNA, or it could protect Rad17 from dephosphorylation. Regardless of the role played by the Rad9-Rad1-Hus1 complex, our in vitro data demonstrate that the recruitment of ATR-ATRIP to ssDNA can lead to its activation toward its substrates on DNA.

RPA is required for the recruitment of Ddc2 to DSBs in vivo. If RPA recruits ATR-ATRIP in vivo, this should be a conserved function detectable in all eukaryotes. We ex-

amined this model in budding yeast, in which DNA damage can be generated in a precise, site-directed manner. A single DSB can be generated by HO at a specific site (29), and the recruitment of Mec1-Ddc2 complex to this damaged site can be detected by chromatin-immunoprecipitation (CHIP) of Mec1 or Ddc2 (8, 9). To analyze the recruitment of Ddc2 to HO-induced DSBs in vivo, we used a strain in which an HO cleavage site was integrated at the telomere of chromosome VII, and the expression of HO was controlled by a galactose-inducible (Gal) promoter (9). To examine the in vivo requirement of RPA for Ddc2 recruitment, we sought to conditionally degrade RPA in cells by fusing Rpa1 to a "degron" tag that confers instability on proteins at 37°C (Fig. 5A) (30). The Ubr1

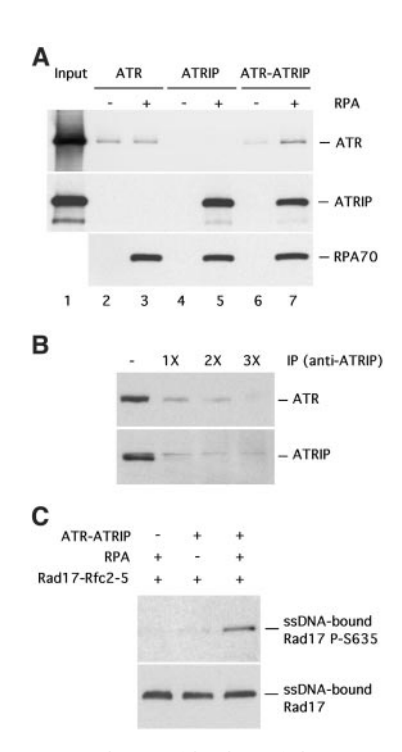


Fig. 4. Stimulation of binding of the ATR-ATRIP complex to ssDNA by RPA. (A) The ATR-ATRIP complex was reconstituted with purified ATR and ATRIP. The biotinylated 75-nt oligomer (5 pmol), either alone or coated with RPA, was incubated with 1 pmol of ATR, ATRIP, or ATR-ATRIP complex. The ATR, ATRIP, and RPA70 bound to DNA were detected by immunoblotting. Input is the total ATR-ATRIP used in the experiment. (B) HeLa cell extracts were subjected to three rounds of immunoprecipitation (IP) with antibodies to ATRIP. The ATR and ATRIP remaining in the extracts after immunoprecipitation were detected by immunoblotting. (C) The biotinylated 75-nt oligomer (5 pmol) was incubated with 1 pmol of the Rad17-Rfc2-5 complex in the presence of ATP. RPA (5 pmol) and ATR-ATRIP (1 pmol) were sequentially added to the reactions as indicated. At the end of reaction, the ssDNA-bound Rad17– Rfc2-5 complexes were retrieved by streptavidin beads, washed, and analyzed by immunoblotting with the antibodies to Rad17 and to P-Ser<sup>635</sup> or Rad17.

ubiquitin ligase was overexpressed from a Gal promoter to facilitate degradation of the degron-tagged Rpa1 (Rpa1-td). In the control cells with wild-type Rpa1, both Ddc2 and Rpa1 were specifically recruited to HOinduced breaks after a 4-hour incubation of cells in a galactose-containing medium at 37°C (Fig. 5B). No enrichment of Ddc2 or Rpa1 was detected at a control locus at TUB1. In the cells expressing Rpa1-td, less Rpa1-td protein was detected at the HO site (Fig. 5B). Binding of Ddc2 to the HO-induced breaks was also substantially diminished in these cells (Fig. 5B). The ssDNA was not degraded in the rpa-td mutant cells, because equal polymerase chain reaction (PCR) signals were detected in the input DNA.

Because depletion of RPA could lead to DNA replication defects that might affect the recruitment of Ddc2, we sought to synchronize cells outside of the S phase and examine the requirement of RPA for Ddc2 recruitment. The enrichment of Ddc2 at the HO-induced break was also reduced in the *rfa1-td* cells arrested at the G<sub>2</sub>/M phases (Fig. 5, C and D), suggesting that the low abundance of RPA (Fig. 5E), rather than the defective DNA replication, is the cause of diminished Ddc2 recruitment. These results strongly suggest that RPA is required for the localization of Mec1-Ddc2 to sites of DNA damage in vivo.

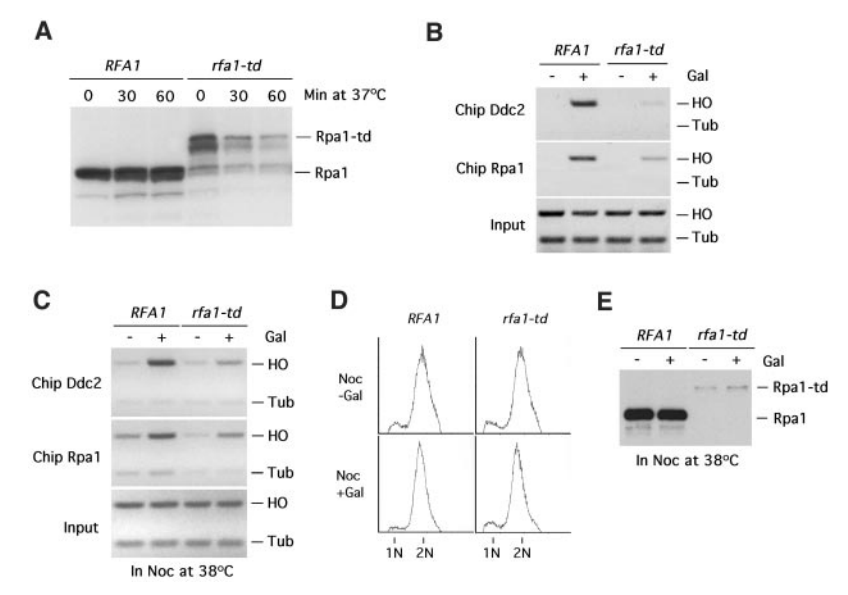
The checkpoint-defective rfa1-t11 mutant is defective in recruiting Ddc2 to ssDNA. The studies described here suggest a model whereby DNA damage generates ssDNA that is bound by RPA, to form an RPA-ssDNA complex that recruits ATR-ATRIP to initiate checkpoint signaling. This model makes the strong prediction that one should be able to generate mutations in RPA that have defective checkpoint signaling. Furthermore, these mutants should display defects in the recruitment of ATR-ATRIP to damage sites and should have a defect in binding to ATRIP. A particular mutation in the large subunit of yeast RPA, rfa1-t11, is a good candidate for such a mutation. rfa1-t11 mutants are proficient for chromosomal DNA replication (31) but are partially defective for the checkpoint response activated by ssDNA at telomeres in the absence of CDC13 function (18).

To study the effects of the *rfa1-t11* mutation on Ddc2 recruitment, we integrated the *rfa1-t11* mutant allele at the endogenous *RFA1* locus in our DSB assay strain and performed CHIP analysis. Wild-type and *rfa1-t11* mutant cells were arrested at the G2/M phases with nocodazole and then cultured in a galactose-containing medium that also contained nocodazole to maintain cell cycle arrest and to induce DSBs. After a 4-hour incubation in galactose, enrichment of approximately equal amounts of Rpa1 at the HO-induced breaks was detected in both *RFA1* and *rfa1-t11* cells (Fig. 6A). This indi-

cates that the *rfa1-t11* mutation does not affect the generation and processing of the HO breaks. In contrast to Rpa1, the amount of increase of Ddc2 at the HO site was reduced by about two-thirds in *rfa1-t11* cells (an increase of 1.1 units) compared to that in *RFA1* cells (an increase of 2.8 units) (Fig. 6A). These results

indicate that the RPA complexes containing Rpa1-t11 (here referred to as RPA-t11) at the HO-induced breaks have reduced ability to recruit Ddc2 in vivo.

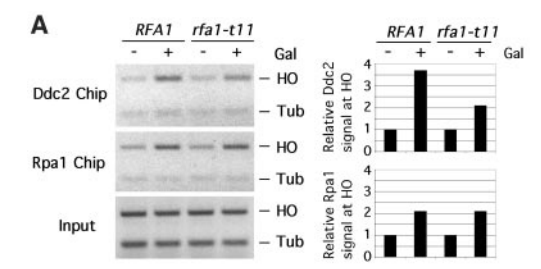
If the binding of Ddc2 to RPA is critical for both recruitment of Ddc2 to damage sites and checkpoint signaling, then the RPA-t11

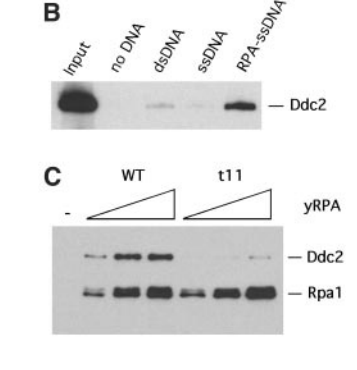


**Fig. 5.** RPA-dependent recruitment of Ddc2 to DNA damage in vivo. **(A)** Yeast cells expressing Rpa1-td or wild-type Rpa1 were grown to log phase in a yeast extract, peptone, and dextrose medium at 23°C, then shifted to 37°C and collected at the indicated times. Extracts derived from the cells were analyzed by immunoblotting with antibodies to Rpa1. **(B)** Yeast cells (Y2302) containing *rfa1-td*, *DDC2-GFP*, *Gal-HO*, and pGal-*UBR1*, or their isogenic cells carrying *RFA1* (Y2303), were grown in a raffinose-containing medium at 37°C for 2 hours. The cells were then cultured in the absence or presence of 2% galactose at 37°C for another 4 hours. The CHIP assay was performed with antibodies to the GFP epitope (for Ddc2-GFP) and to Rpa1. Tub, the PCR product from an unlinked control locus at *TUB1*. **(C)** Wild-type (Y2303) and *rfa1-td* (Y2302) cells were synchronized at the G<sub>2</sub>/M phases with nocodazole (Noc) at 23°C for 3 hours. Cells were then cultured at 38°C for 1 hour before galactose was added to induce HO breaks. Four hours after the addition of galactose, CHIP analysis was performed as in (B). **(D)** DNA content of the cells analyzed in (C). 1N, DNA content of cells in the G<sub>1</sub> phase; 2N, DNA content of cells in the G<sub>2</sub> or M phase. **(E)** Immunoblots of Rpa1 from the cells analyzed in (C).

**Fig. 6.** In vivo and in vitro defects of yeast rfa1-t11 mutants in recruiting Ddc2. (A) Yeast cells (Y2304) containing rfa1-t11, DDC2-GFP, and Gal-HO, or their isogenic cells carrying RFA1 (yJK8-1), were synchronized at the  $G_2/M$  phases with nocodazole for 2 hours. The cells were then cultured in the absence or presence of 2% galactose at 37°C for another 4 hours in nocodazole. The CHIP assay was carried out as in Fig. 5B. The relative enrichments of Ddc2 and

Rpa1 at the HO site were quantified as shown on the right. (B) Human RPA stimulates the binding of Ddc2 to ssDNA. Ddc2 (0.5 pmol) was incubated with streptavidin beads that carried either no DNA or 5 pmol of dsDNA, ssDNA, or human RPA-coated ssDNA. The DNA-bound Ddc2 was retrieved with the beads and analyzed by immunoblotting. (C) Yeast RPA-t11 complexes are defective for recruiting Ddc2 in vitro. Ddc2 was incubated with ssDNA in the absence of RPA or in the presence of various amounts of purified wild-type yeast RPA or RPA-t11 mutant complexes (0.5, 1, or 2 pmol). The DNA-bound Ddc2 and Rpa1 (or Rpa1-t11) were detected by immunoblotting.





complex should be defective for binding Ddc2 in vitro. We expressed Flag-tagged Ddc2 in baculovirus-infected insect cells and purified it by affinity chromatography. In the absence of RPA, Ddc2 bound very weakly to both dsDNA and ssDNA (Fig. 6B). However, the binding of Ddc2 to ssDNA was increased when purified human or yeast RPA was present (Fig. 6, B and C). Therefore, the biochemical mechanism of ATR-ATRIP recruitment to ssDNA appears to be conserved in budding yeast.

To investigate whether RPA-t11 is defective for recruiting Ddc2 to ssDNA, we compared the abilities of purified recombinant yeast RPA and RPA-t11 to recruit Ddc2 in vitro. Like RPA, RPA-t11 could efficiently associate with ssDNA (Fig. 6C). In contrast, the ability of RPA-t11 to recruit Ddc2 to ssDNA was substantially reduced (by about four-fifths) compared to that of wild-type RPA (Fig. 6C). This deficiency is consistent with the impaired checkpoint signaling observed in the *rfa1-t11* mutant and the reduction in recruitment of Ddc2 to sites of DNA damage in vivo.

ssDNA is a common DNA structure generated by interference with DNA replication and various types of DNA repair. Previous genetic studies in yeast have suggested that ssDNA might be part of the signal that activates the DNA damage checkpoint (13). Our results have uncovered RPA-coated ssDNA as a key structure for the activation of the ATR-ATRIP complex in response to DSBs and replication interference (Fig. 7). Furthermore, our data also reveal an analogy between the damage response in eukaryotic cells and that in prokaryotes. In bacteria, ssDNA generated by damage processing is coated with RecA and serves as a signal for the SOS response (32). Although eukaryotes have developed more elaborate mechanisms to respond to DNA damage, the use of ssDNA as a signal of damaged DNA is evolutionarily conserved from bacteria to humans.

Fig. 7. A model for RPA regulation of ATR-ATRIP in response to DSBs and DNA replication interference. The Rad17 complex shown in the model is only an example of the many substrates of ATR-ATRIP that are recruited to DSBs or stressed replication forks. Although some ATR-ATRIP may associate in lower amounts with unperturbed replication forks, the recruitment of ATR-ATRIP to replication forks and the phosphorylation of ATR substrates are stimulated by replication interference.

forks that function normally during the S phase, massive activation of the ATR-ATRIP signaling pathway is not observed. This may be simply an issue of sensitivity. Alternatively, it is possible that the extent of RPA binding during normal replication is transitory and insufficient to elicit an ATR-ATRIP response or that the RPA bound during normal replication is protected from ATRIP binding. When replication forks are under stress or encounter DNA lesions, persistent, longer stretches of ssDNA could be generated by the stalling of polymerases, the uncoupling of helicases and polymerases, or both (Fig. 7). This might allow more ATR-ATRIP to be recruited to the hindered replication forks or the sites of DNA damage. Furthermore, the loading of multiple RPAs to longer ssDNA might have a synergistic effect on ATR-ATRIP recruitment, as we detected in vitro. In budding yeast, the length of ssDNA at replication forks increases in the presence of HU (34). In Xenopus extracts, increased amounts of RPA and ATR are detected on chromatin treated with aphidicolin, UV, or methyl methane sulfonate (35, 36). In human cells, increased amounts of RPA associated with chromatin after DNA damage (Fig. 1A). In addition to DNA replication, various DNA repair or recombination processes, such as homologous recombination, nucleotide excision repair, and base excision repair, also generate ssDNA (37). Many types of DNA lesions can induce DNA synthesis independently of the cell cycle-regulated DNA replication. Our finding that RPAcoated ssDNA is sufficient to recruit ATR-

The presence of RPA-coated ssDNA at

replication forks might bring ATR-ATRIP to

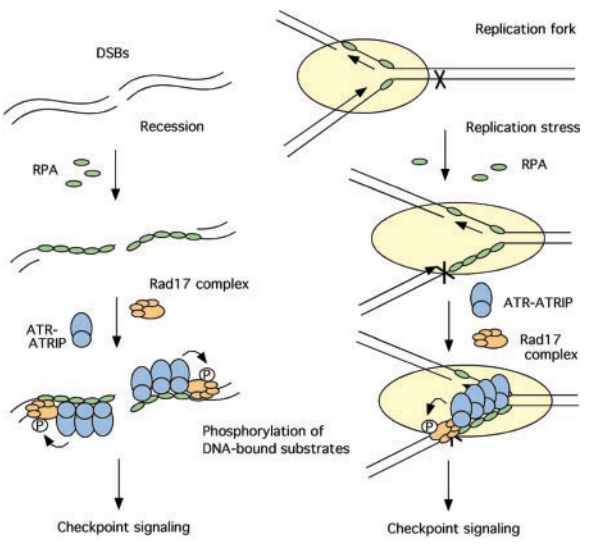
these complexes to monitor DNA synthesis.

Indeed, Xenopus RPA is required for the

initiation of DNA replication and the con-

comitant ATR binding to chromatin (33).

Although RPA associates with replication



ATRIP raises the possibility that DNA repair processes may also cause the activation of ATR signaling. For example, in *Xenopus* extracts, etoposide-induced DNA damage triggers prereplication complexindependent DNA synthesis and recruits both RPA and ATR onto chromatin (38). The results from this study may provide a molecular basis for damage recognition by ATR-ATRIP and explain the broad spectrum of ATR-mediated damage responses.

It was recently reported that Ddc2 binds to the ends of DSBs and thereby recruits Mec1 to the sites of DNA damage (25). However, many types of DNA replication interference that do not lead to substantial DSBs can activate the checkpoint through Mec1-Ddc2. Furthermore, although the induction of HO breaks is very rapid in yeast, Mec1-Ddc2 is not detected at the breaks until a few hours after the cleavage, when ssDNA is generated at these sites (8, 9). We find that purified Ddc2 and ATRIP have a low affinity for DSBs in vitro relative to RPA-ssDNA complexes. Our results do not rule out direct sensing of DSBs or other DNA structures by ATR-ATRIP complexes, but support a more prominent role for ssDNA in their recruitment to sites of DSBs and replication interference.

The mechanism by which ATR is activated by replication stress and DNA damage is a key question for the understanding of cellular stress and damage responses. Unlike ATM, ATR isolated from damaged cells does not display increased specific activity in kinase assays (20). Rather, our results indicate that an apparent activation may be achieved by the simultaneous enrichment of ATR-ATRIP and its substrates at the sites of DNA damage. If this is the case, then any mechanism that localizes ATR-ATRIP to another protein could promote substrate phosphorylation.

The localization of ATR-ATRIP to sites of DNA damage alone is not sufficient to fully activate the checkpoint response. The RFC-like Rad17 complex and the PCNA-like Rad9-Rad1-Hus1 complex take part in the recognition of DNA damage. These complexes might have important roles in recruiting the ATR substrates, organizing the protein-DNA complexes at the damage sites, and allowing ATR to gain further access to substrates. The elucidation of how ATR-ATRIP, Rad17, and Rad9-Rad1-Hus1 complexes interact on damaged DNA to amplify damage signals will be a critical focus for future studies on checkpoint signaling.

# **References and Notes**

- 1. B. B. Zhou, S. J. Elledge, Nature 408, 433 (2000).
- 2. R. T. Abraham, Genes Dev. 15, 2177 (2001).
- D. Cortez, S. Guntuku, J. Qin, S. J. Elledge, Science 294, 1713 (2001).

- R. J. Edwards, N. J. Bentley, A. M. Carr, *Nature Cell Biol.* 1, 393 (1999).
- V. Paciotti, M. Clerici, G. Lucchini, M. P. Longhese, Genes Dev. 14, 2046 (2000).
- 6. J. Rouse, S. P. Jackson, EMBO J. 19, 5801 (2000).
- T. Wakayama, T. Kondo, S. Ando, K. Matsumoto, K. Sugimoto, Mol. Cell. Biol. 21, 755 (2001).
- 8. T. Kondo, T. Wakayama, T. Naiki, K. Matsumoto, K. Sugimoto, *Science* **294**, 867 (2001).
- J. A. Melo, J. Cohen, D. P. Toczyski, Genes Dev. 15, 2809 (2001).
- 10. L. Zou, D. Ćortez, S. J. Elledge, *Genes Dev.* **16**, 198 (2002)
- 11. D. Lydall, T. Weinert, Science **270**, 1488 (1995).
- A. Pellicioli, S. E. Lee, C. Lucca, M. Foiani, J. E. Haber, Mol. Cell 7, 293 (2001).
- 13. M. B. Vaze et al., Mol. Cell 10, 373 (2002).
- 14. M. S. Wold, Annu. Rev. Biochem. **66**, 61 (1997).
- G. S. Brush, D. M. Morrow, P. Hieter, T. J. Kelly, *Proc. Natl. Acad. Sci. U.S.A.* 93, 15075 (1996).
- G. S. Brush, T. J. Kelly, Nucleic Acids Res. 28, 3725 (2000).
- M. P. Longhese, H. Neecke, V. Paciotti, G. Lucchini, P. Plevani, Nucleic Acids Res. 24, 3533 (1996).
- 18. H. S. Kim, S. J. Brill, Mol. Cell. Biol. 21, 3725 (2001).

- E. I. Golub, R. C. Gupta, T. Haaf, M. S. Wold, C. M. Radding, *Nucleic Acids Res.* 26, 5388 (1998).
- 20. R. S. Tibbetts *et al.*, *Genes Dev.* **14**, 2989 (2000).
- 21. L. Zou, S. J. Elledge, unpublished data.
- Q. Liu et al., Genes Dev. 14, 1448 (2000).
   L. A. Henricksen, C. B. Umbricht, M. S. Wold, J. Biol.
- Chem. **269**, 11121 (1994). 24. J. Rouse, S. P. Jackson, *Mol. Cell* **9**, 857 (2002).
- K. Unsal-Kacmaz, A. M. Makhov, J. D. Griffith, A. Sancar, *Proc. Natl. Acad. Sci. U.S.A.* 99, 6673 (2002).
- L. A. Lindsey-Boltz, V. P. Bermudez, J. Hurwitz, A. Sancar, *Proc. Natl. Acad. Sci. U.S.A.* 98, 11236 (2001).
- 27. S. Bao et al., Nature 411, 969 (2001).
- 28. S. Post et al., Proc. Natl. Acad. Sci. U.S.A. 98, 13102 (2001).
- 29. L. L. Sandell, V. A. Zakian, Cell 75, 729 (1993).
- R. J. Dohmen, P. Wu, A. Varshavsky, Science 263, 1273 (1994).
- K. Umezu, N. Sugawara, C. Chen, J. E. Haber, R. D. Kolodner, *Genetics* 148, 989 (1998).
- M. D. Sutton, B. T. Smith, V. G. Godoy, G. C. Walker, Annu. Rev. Genet. 34, 479 (2000).
- Z. You, L. Kong, J. Newport, J. Biol. Chem. 277, 27088 (2002).

- J. M. Sogo, M. Lopes, M. Foiani, Science 297, 599 (2002).
- 35. W. M. Michael, R. Ott, E. Fanning, J. Newport, *Science* **289**, 2133 (2000).
- P. J. Lupardus, T. Byun, M. C. Yee, M. Hekmat-Nejad,
   K. A. Cimprich, *Genes Dev.* 16, 2327 (2002).
- R. D. Wood, M. Mitchell, J. Sgouros, T. Lindahl, Science 291, 1284 (2001).
- 38. V. Costanzo et al., Mol. Cell 11, 203 (2003)
- 39. We thank P. Sung and S. Kowalczykowski for the purified human and yeast RPA used in some experiments; D. Toczyski, R. Kolodner, D. Cortez, S. Brill, J, Hurwitz, H. Rao, and E. Friedberg for reagents; and D. Liu for technical assistance. L.Z. is a Fayez Sarofim fellow of the Damon Runyon Cancer Research Fund. S.J.E. is funded by NIH (grant no. GM44664) and is an investigator with the Howard Hughes Medical Institute and the Welch Professor of Biochemistry.

# Supporting Online Material

www.sciencemag.org/cgi/content/full/300/5625/1542/

Materials and Methods

13 February 2003; accepted 2 May 2003

# REPORTS

# Entangled Macroscopic Quantum States in Two Superconducting Qubits

A. J. Berkley,\* H. Xu, R. C. Ramos, M. A. Gubrud, F. W. Strauch, P. R. Johnson, J. R. Anderson, A. J. Dragt, C. J. Lobb, F. C. Wellstood

We present spectroscopic evidence for the creation of entangled macroscopic quantum states in two current-biased Josephson-junction qubits coupled by a capacitor. The individual junction bias currents are used to control the interaction between the qubits by tuning the energy level spacings of the junctions in and out of resonance with each other. Microwave spectroscopy in the 4 to 6 gigahertz range at 20 millikelvin reveals energy levels that agree well with theoretical results for entangled states. The single qubits are spatially separate, and the entangled states extend over the 0.7-millimeter distance between the two qubits.

Most research on quantum computation (I) using solid-state systems has been focused on the behavior of single isolated quantum bits (qubits) (2-9). For example, progress in the last 2 years on single superconducting qubits has included the observation and control of states formed from quantum superpositions (3-9). In addition to quantum superpositions, quantum computation also requires the entanglement of multiple qubits (10). Entanglement is critical for enabling a quantum computer to be exponentially faster than a classical one (11) and means that the state of one qubit depends inextricably on the state of another qubit. Recently, entanglement in a superconducting charge-

Center for Superconductivity Research, Department of Physics, University of Maryland, College Park, MD 20742, USA.

\*To whom correspondence should be addressed. E-mail: berkley@physics.umd.edu

based two-qubit system with an overall size of a few micrometers has been reported (3). We describe a different superconducting coupled qubit system with qubits separated by a distance that is hundreds of times larger. Our microwave spectroscopic measurements (12, 13) show clear evidence for entangled states in this macroscopic system.

Each of our qubits is formed by a single current-biased Josephson junction (14). The behavior of such a junction is analogous to a particle of mass  $C_j$  that moves in a tilted washboard potential (Fig. 1A) (15)

$$U(\gamma) = -I_{c}(\Phi_{0}/2\pi)\cos(\gamma) - I_{b}\gamma\Phi_{0}/2\pi \quad (1)$$

where  $I_{\rm b}$  is the bias current flowing through the junction,  $I_{\rm c}$  is the critical current,  $C_{\rm j}$  is the junction capacitance,  $\Phi_0 = 2.07 \times 10^{-15}$  T-m<sup>2</sup> is the flux quantum, and  $\gamma$  is the phase difference of the quantum mechanical wavefunction across the junction (15). We note

that  $\gamma$  is a collective degree of freedom for the roughly 109 paired electrons in the metal from which the qubit is constructed (16) and  $d\gamma/dt$  is proportional to the voltage across the junction. Quantization of this system leads to metastable states that are localized in the potential well and have well-defined energies (Fig. 1A). The lifetimes of the states can be long, provided an appropriate isolation network prevents the junction from dissipating energy to its bias leads (2, 4, 5, 12, 13). At bias currents  $I_{\rm b}$  slightly lower than  $I_{\rm c}$ , there are only a few states trapped in the well, and the barrier is low enough to allow escape by quantum tunneling (17, 18) to a set of continuum states that exhibit an easily detectable direct current (DC) voltage.

We coupled two junction qubits together by using a capacitor  $C_c$  (Fig. 1B) (19-21). The strength of the qubit-qubit coupling is set by  $C_c/(C_i + C_c)$ , which for our qubits is about 0.1. When the current through one qubit is adjusted to produce an energy level spacing equal to that in the other qubit, the capacitive coupling leads to mixing of the uncoupled states and a lifting of the energy degeneracy (19). Near this "equal-spacing" bias point, the three lowest levels of the system are the ground state |00\range and two excited states  $(|01\rangle \pm |10\rangle)/\sqrt{2}$ . Here the notation  $|01\rangle$  indicates, for example, that the first qubit is in its ground state  $|0\rangle$  and the second is in its first excited state |1\). These two-qubit excited states are entangled; when qubit 1 is found in the ground state  $|0\rangle$ , then qubit 2 is found in the excited state  $|1\rangle$ , and vice versa.

Our qubits are fabricated with the use of a Nb-AlO $_x$ -Nb thin film trilayer process on 5 mm by 5 mm Si chips (Fig. 1C). Each qubit is a 10  $\mu$ m by 10  $\mu$ m Josephson junction. The cou-